AIAA JOURNAL
Vol. 44, No. 12, December 2006

Static and Dynamic Delamination of Foam Core Sandwich Members

Srinivasan Sridharan* and Yupeng Li†
Washington University in St. Louis, St. Louis, Missouri 63130

DOI: 10.2514/1.20525

Delamination of sandwich columns is studied using simple cohesive layer models, one with a finite thickness and the other with zero initial thickness, designated, respectively, as user supplied material and user supplied element models. The latter model predicts accurately the test results of delamination of a facing sheet of a sandwich member and is seen to be more accurate than the former which predicts an earlier termination of crack growth. The user supplied elements model is applied to sandwich columns under compression. Both static and dynamic delamination problems are studied. The static problem involves monotonically increasing end-shortening, whereas the dynamic delamination is studied under constant end-shortening with delaminations suddenly triggered. It is seen that for end-shortening values close to that causing delamination buckling in the static case, the dynamic delamination is abrupt and total. Two typical cases of sandwich columns, one relatively stout and the other somewhat slender, are studied and they offer interesting contrasts with the corresponding static behavior.

Nomenclature

d	=	depth of specimen
E_2	=	transverse Young's modulus of the cohesive layer
E_x, E_y, E_z	=	longitudinal, transverse, out-of-plane Young's moduli, respectively
E_f, E_c	=	Young's moduli of fiber and core, respectively
G_{xy}, G_{xz}, G_{yz}	=	shear moduli
G_I	=	modal 1 component (opening mode) of strain energy release rate
G_{Ic}	=	mode 1 critical strain energy release rate
h	=	thickness of facing sheet
h_o	=	initial thickness of cohesive layer
h_c	=	current thickness of cohesive layer
L	=	length of specimen
ℓ_o	=	initial crack length
ℓ_{cr}	=	current crack length
P	=	axial compression
t	=	process zone thickness
w	=	width of the specimen
x, y	=	coordinates with respect to global coordinate system
u, v	=	displacements with respect to global coordinate system
α	=	damping factor
Δ	=	end shortening
$\Delta\delta_n$	=	incremental normal relative displacement
$\Delta\varepsilon_n$	=	increments of normal strain and shear strain, respectively
δ_n, δ_t	=	relative displacements in normal and tangential directions, respectively
δ_{np}, δ_{tp}	=	proportional limits of δ_n, δ_t, respectively
ν_{xy}, ν_{xz}, ν_{yz}	=	Poisson's ratio
ν_f, ν_c	=	Poisson's ratio of fiber and core
$\sigma_{\max}$, $\tau_{\max}$	=	transverse and shear strengths of cohesive layer, respectively
σ_n	=	current normal stresses

Received 14 October 2005; accepted for publication 20 August 2006.

*Corresponding author, Professor, Department of Civil Engineering, Campus Box 1130, 1 Brookings Drive; ssrid@seas.wustl.edu. Senior Member AIAA.

†Research Assistant, Department of Civil Engineering; currently Intel Corporation, Chandler, Arizona.

Introduction

AN often encountered failure mode of sandwich structural components is the core facing debonding. Once such debonding occurs, the integrity of the structure is compromised and a significant reduction in the stiffness and the load carrying capacity occurs. A sandwich member under compression is more delamination-sensitive as the delaminated skin tends to buckle, thus accentuating the risk of delamination growth. It appears that a member under compression when hit by a projectile can experience sudden and total delamination failure. A lateral impact can trigger delamination at the opposite facing-core interface which can grow dynamically under compression. Such a phenomenon has been observed in tests on laminated composites [1] (Chai et al., 1983) and is investigated in the present paper in the context of sandwich composite members.

Under quasi-static loading, the extent of the growth of delamination depends upon the overall bending stiffness of sandwich beam as well as the bending stiffness of the delaminating facing sheet. As the structure bends in an overall sense, delamination crack tends to close whether the member bends away or towards the delaminated facing. Thus, the overall bending inhibits the growth of delamination which may come to a standstill despite a continuing increase in the load carried.

Previous experience [2,3] has indicated that the delamination failure in sandwich members is principally in mode 1 (opening mode) with shear playing a negligibly small role. Thus, the most significant parameter required for tracing delamination growth is G_{Ic}. To trace the delamination growth without interference by the user, a cohesive layer model interposed between the facing and the core is employed. There exist numerous papers on the application of cohesive layer models to tracing delamination growth [see for example, Ortiz and Pandolfi [4] (1999), Yu [5] (2001), and Alfano and Crisfield [6] (2001)]. The model comes in handy especially in the context of dynamic response of the member when the crack grows in an unstable manner. The authors have developed two types of the model [7] in a highly simplified form which are used in conjunction with a widely used nonlinear finite element program [8,9]:

1) UMAT model: The cohesive layer is of finite thickness and represented by a layer of elements of a type available in a standard finite element package, but with *user supplied material* properties, hence called the UMAT [8] model. The material property that is

significant here is the relationship between incremental stress and incremental strain in the transverse direction. Note, cohesive layer models with finite thickness have been used by several investigators, see for example, Sprenger et al. [10].

2) UEL model: The cohesive layer has zero thickness initially and is represented by a set of *user supplied elements*. The user has to define the nodal forces and the current stiffness of the elements based on the relative displacement suffered by the element between its two separating surfaces. This is a more common version of the cohesive layer model [6].

It has been recently found [7] that these two models can differ in their predictions of delamination growth and thus a comparative study in the light of experimental results appears warranted. In the present work, a quasi-static sandwich delamination problem is investigated using the two models. The UEL model is seen to be clearly superior in its performance in tracing extensive delamination of the facing-core. The delamination of sandwich columns under compression is next studied under the following conditions: 1) static loading involving monotonically increasing end-shortening, and 2) a fixed end-shortening with dynamically triggered delamination. Some interesting contrasts in the behavior are observed in the two scenarios.

Description of the Cohesive Layer Models

UMAT Model

This model employs a constitutive relationship in the form of a stress–strain relationship of the cohesive layer. The stresses and strains of the cohesive layer element are referred to axes which rotate with the element. Thus, the effect of rigid body rotations is eliminated in the incremental strain-displacement relations. In the present context, only the normal stress–strain relationship in the transverse direction is of pertinence and other relationships are assumed linear elastic. Poisson's ratio is set to zero. For simplicity, a bilinear elastic relationship consisting of a linear elastic phase (given by the modulus E_2) followed by a phase in which stress remains constant at $\sigma_{\max}$ (similar to "elastic-perfectly plastic" response) is assumed. No unloading phase is considered, i.e., in effect unloading is deemed to be abrupt, as soon as the failure criterion for the cohesive layer element is satisfied. The values of E_2 and $\sigma_{\max}$ must be representative of the core material through which the crack propagates. The other significant parameter is the initial thickness of the cohesive layer. Ideally, h_o must be based on the observed dimensions of the process zone [11] (of the order tenths of a millimeter). For reliability, the cohesive layer element, usually the lowest order 4-noded element, must have an aspect ratio close to unity, and so the smaller the value of h_o the higher the computational cost. Usually a compromise is sought.

The cohesive material response calculations are performed in a module (UMAT) attached to the input program of Abaqus. A 4-noded plane strain/plane stress element with reduced integration is selected for the cohesive layer for the 2-D problems studied here. Because reduced integration is used, a single integration point represents the whole element. The incremental strain is computed based on the current cohesive layer thickness, and so the total strain is approximately logarithmic. As the nonlinear analysis proceeds, the value of G_I is accumulated as in

$$G_I = \sum_{i=1}^{m} \sigma_n h_c \Delta\varepsilon_n \tag{1}$$

where G_I is accumulated by summation up to the current (mth) load increment. Failure is deemed to occur as soon as the fracture criterion, $G_I \geq G_{Ic}$, is satisfied. The main program supplies the incremental strains which are based on the current (updated) dimensions and the user supplied material subroutine (UMAT) returns to the main program the material stiffness matrix and the stresses at the integration point.

UEL Model

This cohesive layer model has zero initial thickness and is represented as a line in the undeformed state. The notion of strain is suspended and relative displacements of the nodes of the element are used to characterize the deformation and compute the nodal forces. Elements in the model are 4-noded with two displacement degrees of freedom per node. The deformation is characterized in terms of the current averaged normal and tangential relative displacements. The normal and shear stress components in the element are related to δ_n and δ_t, respectively, via bilinear elastic relationships consisting of a linearly varying stress phase and a constant stress phase. The proportional limits of δ_n and δ_t are prescribed taking into consideration the stiffness of the material and the thickness of the process zone. They can be estimated as

$$\delta_{\text{np}} \approx \frac{\sigma_{\max}}{E_2} t, \quad \delta_{\text{tp}} \approx \frac{\tau_{\max}}{G_{12}} t$$

where G_{12} is the shear modulus of the cohesive material. Further, δ_{np} must be chosen to be sufficiently small so that the elastic strain energy contribution is small compared with the cohesive strain energy in the layer. Nodal forces and the stiffness matrix are found in terms of the stress state in the element. These are transformed to the global axes and returned to the main program. The total strain energy stored per unit area in the opening mode in the element is given as a sum of incremental contributions as follows:

$$G_I = \sum_{i=1}^{m} \sigma_n \Delta\delta_n \tag{2}$$

where the summation is over all the increments up to and including the current one. Failure is deemed to occur as soon as the following fracture criterion is satisfied: $G_I \geq G_{Ic}$.

Figure 1 shows a typical element ABCD and its deformed configuration A′B′C′D′; the original coordinates and displacements are given with appropriate subscripts. Note, A and B coincide with D and C, respectively, in the undeformed configuration, shown separately for clarity. The main program supplies for each increment of loading the current nodal displacements (those at the end of the previous loading increment) and their corresponding increments for each iteration with reference to the global coordinate system.

If θ is the averaged orientation of the element with reference to the x-axis, then

$$\tan\theta = \frac{y_2 - y_1}{x_2 - x_1} \tag{3}$$

where

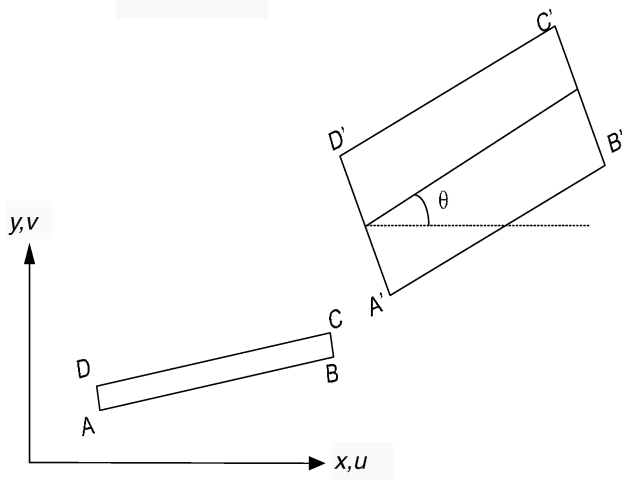

Fig. 1 Typical element ABCD and its deformed configuration A′B′C′D′.

$$y_2 = \frac{(y_C + v_C) + (y_B + v_B)}{2}; \qquad y_1 = \frac{(y_D + v_D) + (y_A + v_A)}{2}$$
$$x_2 = \frac{(x_C + u_C) + (x_B + u_B)}{2}; \qquad x_1 = \frac{(x_D + u_D) + (x_A + u_A)}{2} \tag{4}$$

The current relative displacements in the normal and tangential directions in the current configuration of the element are then computed by transformation

$$\delta_n = (v_2 - v_1)\cos\theta - (u_2 - u_1)\sin\theta$$
$$\delta_t = (v_2 - v_1)\sin\theta + (u_2 - u_1)\cos\theta \tag{5}$$

where

$$u_1 = \frac{u_A + u_B}{2}; \qquad u_2 = \frac{u_C + u_D}{2}$$
$$v_1 = \frac{v_A + v_B}{2}; \qquad v_2 = \frac{v_C + v_D}{2} \tag{6}$$

From the assumed stress-displacement relationship, the stress components σ_n and τ carried by the element are determined. These in turn are employed to determine the nodal forces in terms of the element length. The tangential stiffness matrix for the element is set up by appropriate differentiation. The current nodal forces and the tangential stiffness matrix are then transformed to the global axes and returned to the main program. Note that the nodal forces are updated for every iteration.

Evaluation of Performance of the Models Using a Test Case

Li performed tests [12] on a sandwich member with a length of 210 mm, completely restrained along one of its facings (top facing sheet in Fig. 2) and loaded uniformly across its width at one end of the other facing (bottom, in Fig. 2). The specimen carried a preimplanted delamination of 51 mm. Of the three groups of specimens tested, only one group, identified as "KKV sandwich," exhibited propagation of crack along the interface (about 0.5 mm below the face/core interface). We consider here a case where the load application is transverse, i.e., 90 deg to the axis of the member. The geometry, the loading, and the boundary conditions of the test specimen are indicated in Fig. 2.

The facing sheets are made up of E-glass/vinyl ester, whereas the core material is H200 Divinycell PVC foam. Table 1 lists the elastic properties of the materials. Here, we use the averaged elastic properties as determined from compression and tension tests. (The most important property is the effective modulus in the longitudinal direction which determines the slope of the initial linear phase before crack initiation which varied from 23.2 GPa in compression to 26.0 GPa in tension; an average value of 24.6 GPa is used for the comparison with experiment.)

Table 1 Material properties of Li's specimen [12]

Material property	Face sheet	Core
Young's moduli, GPa: E_x, E_y, E_z	24.6, 11.8, 13.5	0.165, 0.263, 0.165
Poisson's ratios, υ_{xy}, υ_{xz}, υ_{yz}	0.31, 0.533, 0.446	0.32, 0.32, 0.32
Shear moduli, GPa: G_{xy}, G_{xz}, G_{yz}	3.78, 9.19, 3.74	0.0644, 0.0644, 0.0644
Critical strain energy release rate mode 1: G_{Ic}, J/m^2	1270	

Selection of Parameters: General

The critical strain energy release rate in the opening mode as measured by Li [12] is 1.270 N/mm. The next in order of importance is the selection of maximum stress. This value controls the point at which delamination growth initiates, but not so much the delamination growth phase [6,7]. The maximum stress must, however, be representative of the tensile strength of the material in which the crack propagates. Given the complexities of actual crack propagation in the specimen [12] and the fact that our cohesive model is somewhat simplistic, in that it does not include an strain-softening branch, we proceed by taking $\sigma_{\max}$ equal to the material strength of the foam and evaluating the sensitivity of the response to $\sigma_{\max}$. The tensile strength of the core material (H200 Divinycell foam) is about 6 MPa (Abot [13]).

Modeling Details

The finite element model consisted of 4-noded plane strain elements with reduced integration (CPE4R) throughout and the sizes of the element chosen are indicated in Fig. 3. The typical size of the element in the direction of the crack is 0.25 mm and thus, in each layer, there were 840 elements end-to-end. (A trial run with a coarser mesh with 0.50 mm size gave essentially the same results.) Loading was introduced by prescribing the deflection at the point of application of the load and computing the reaction thereof. A total deflection of 30 mm was reached in 1000 increments.

Li [12] (2000) studied the problem experimentally by a repeated sequence of loading up to incipient crack growth, letting the crack grow to a certain extent, unloading fully, and reloading as before. Figure 4 displays the key points taken from these experimental results which the authors have taken the liberty of replotting, ensuring the characteristics passed through the origin (elimination of zero error) but maintaining the slopes of the reloading characteristics and the loads recorded at the crack initiation at the end of each loading phase. (The peak point coincides with initiation of crack

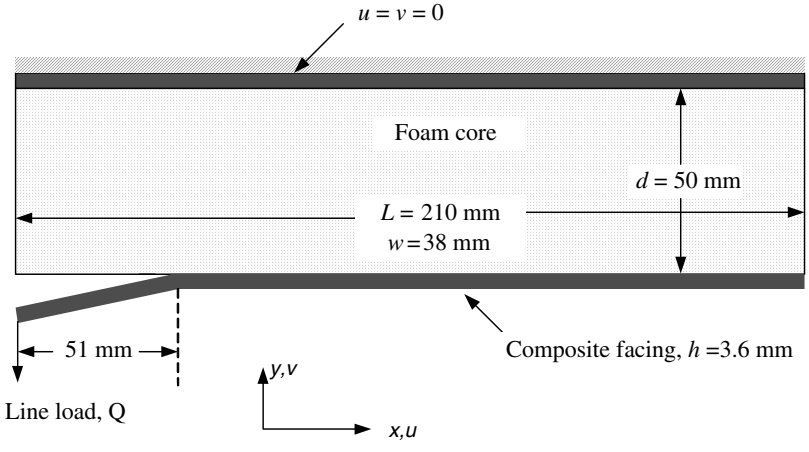

Fig. 2 Test configuration of Li's sandwich specimen [12].

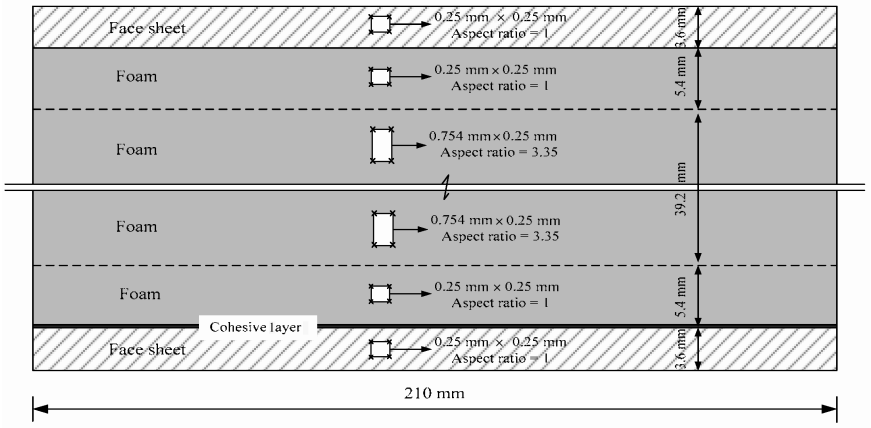

Fig. 3 Finite element configuration (not to scale).

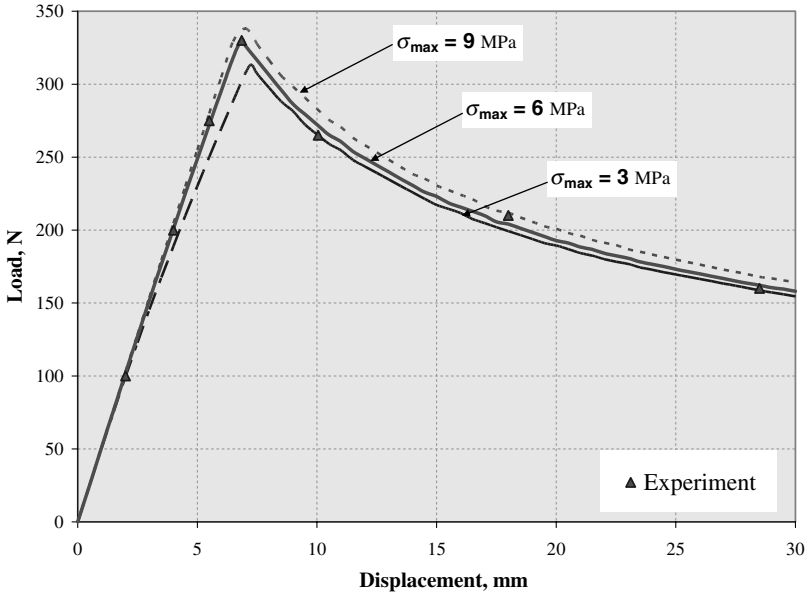

Fig. 4 Simulation results from UEL model vs experimental results.

growth and other experimental data points on the unloading branch correspond to crack initiation upon reloading.)

Performance of the UEL Model

As already mentioned, the prediction of crack initiation point depends on the $\sigma_{\max}$ selected. Thus, three values were selected for $\sigma_{\max}$, viz., 3, 6, and 9 MPa, respectively. The first and the last value being 50% less and 50% more, respectively, from the nominal strength of the core material, viz., 6 MPa. The other parameters of the model are $\tau_{\max} = 20.0$ Mpa, $\delta_{\text{np}} = 1.\text{e} - 2$, $\delta_{\text{tp}} = 1.\text{e} - 3$, $G_{Ic} =$ 1.270 N/mm, and G_{IIc} is set at an arbitrarily high value.

It is apparent that the value of 3 MPa for $\sigma_{\max}$ is too small, for the corresponding cohesive layer behavior is too compliant in the vicinity of crack initiation; the value of 9 MPa slightly overestimates the load corresponding to crack initiation. Thus, as far as foam core sandwich members are concerned, we may conclude that reasonable delamination predictions can be obtained using the present UEL model, by selecting for $\sigma_{\max}$ close to the actual strength of the core. It is interesting to note that the rate of delamination growth is independent of $\sigma_{\max}$, which, however, does control the length of the cohesive zone. Thus, its influence prevails up to the initial formation of the cohesive zone; thereafter, the cohesive zone moves forward as the crack tip element fails (a process controlled by energy accumulated by the element and released upon failure). Figure 5 shows the stress distribution around the crack tip for the case with $\sigma_{\max} = 6$ MPa. It is seen that the model preserves the features of a sharp crack, with a highly localized stress concentration with little damage upstream of the crack.

Performance of the UMAT Model

The finite element mesh configuration selected for the analysis is similar to the one used for the UEL model, except for the mesh size in the longitudinal direction which is now 0.5 mm. Several values of

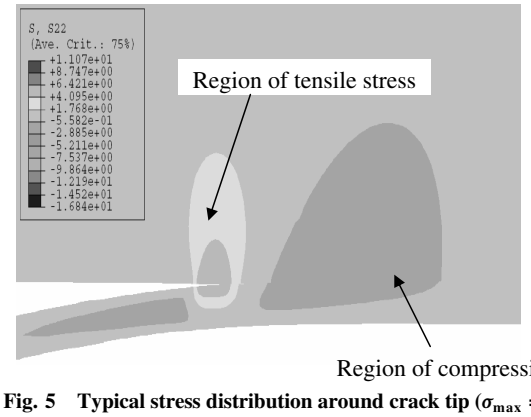

Fig. 5 Typical stress distribution around crack tip ($\sigma_{\max} = 6$ MPa).

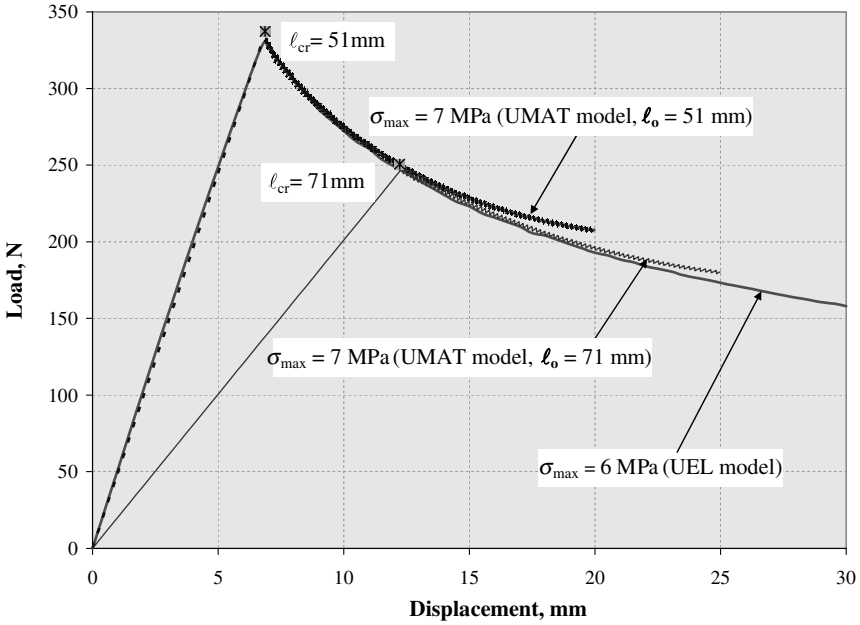

Fig. 6 Comparison between UEL and UMAT results.

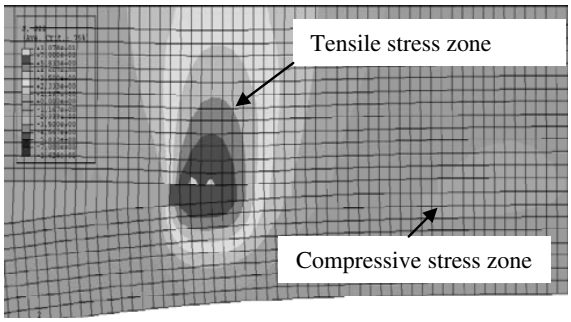

Fig. 7 Stress distribution around crack tip.

strength were investigated and it was anticipated that the strength parameter for the UMAT model must be higher than that of the UEL model to compensate for the influence of compressive stress developing in the cohesive layer upstream of the crack, communicated to the crack tip through the cohesive layer of finite thickness. However, the analysis revealed that the cohesive zone (that part of the cohesive layer which is in tension starting from the crack tip) was sufficiently long (12 elements in length) so that the influence of compression further upstream is not significant.

Figure 6 shows the simulation results for a typical case with $\sigma_{max} = 7$ MPa, where the displacement under the load is plotted against the load carried. The results for an initial crack length of 51 mm are similar to that obtained previously with the UEL model, up to a point past the crack initiation (the peak load) and some significant crack growth (20 mm). But, thereafter, the crack growth shuts off, the load levels off and begins to increase (not shown). There is no reason to suppose that such a prediction has any validity to it, and in fact is shown later in this section to be due to an intrinsic deficiency of the model.

Consider what happens when an initial crack length of $\ell_o >$ 51 mm is assumed, say 71 mm. The initial linear part of the load-displacement characteristic has a smaller slope and crack initiation occurs at a point which lies on or close to the intersection of this line with the unloading characteristic associated with $\ell_o = 51$ mm. But the unloading characteristic associated with $\ell_o = 71$ mm deviates from that associated with an initial crack length of 51 mm and lies closer to that given by UEL model with $\sigma_{max} = 6$ MPa, and is therefore in good agreement with experimental result. However, this characteristic too gradually deviates from the correct result with the crack growth shutting off once again. It is clear, therefore, that the UMAT model, though capable of predicting crack initiation correctly, gradually loses its ability to predict continued crack growth.

Figure 7 shows the magnified image of stress distribution in the close vicinity of the crack tip for the case with $\ell_o = 51$ mm when the crack opening displacement measured at the point of load application is 25 mm. At this instant, crack has progressed to a length of 101 mm. It is seen that the cohesive layer stress, which is tensile in the vicinity of the crack tip, gradually diminishes to zero as we travel upstream of the crack and changes to compression.

Figures 8a and 8b show magnified views of deformed configuration in the vicinity of the crack tip corresponding to the following two cases, respectively:

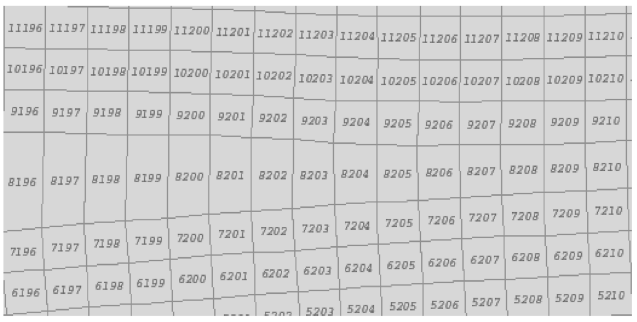

a) Case 1

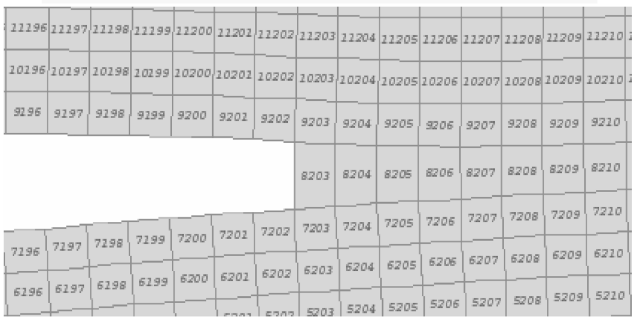

b) Case 2

Fig. 8 Deformed configuration amplified near the crack tip for a) case 1, and b) case 2.

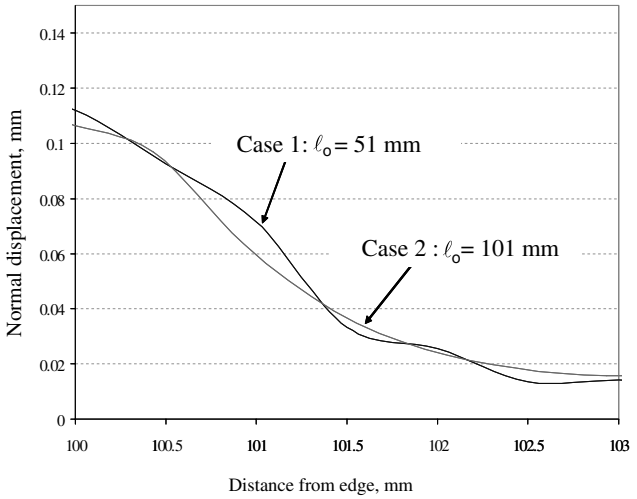

Fig. 9 Displacements along the bottom surface of the cohesive elements.

1) The current crack length of 101 mm is reached after a crack extension of 50 mm from the initial crack length of 51 mm.

2) The initial crack length is taken as 101 mm and the crack tip element is on the verge of failure ($\ell_{cr} = \ell_o = 101$ mm).

The pattern of deformation of the cohesive layer is not the same in the two cases, though the contrast is not altogether clear. Figure 9 plots to a much larger scale the deformation of the bottom surface of the cohesive elements close to the crack tip for the two cases. Note that the downward deflections are plotted above the x-axis in the figure.

There are two features that may be observed in Figs. 7–9.

1) The presence of compressive zone upstream of the crack tip as already noted.

2) In case 1 the depth of the cohesive layer reduces as we travel upstream from the crack tip and a "neck" (a region of slightly reduced depth compared with neighboring regions on either side) appears. This is in contrast to the case 2, which exhibits a smooth variation of the cohesive layer. In Fig. 9, the contrast between the deformation of the bottom surface of the cohesive elements in the two cases is brought home. In case 1, the surface is undulating with a neck formed close to the crack tip.

It is clear that item 2 must be the result of what transpires during the failure of cohesive elements and the accompanying crack extension. If an observer is stationed at the crack tip and moves with it, he/she can see the deformation of the cohesive layer upstream of the crack getting continuously, albeit very subtly, modified. As each element fails, certain force is released onto the delaminated sheet which rotates so as to compress the cohesive layer upstream, causing the formation of a neck. Once a neck of certain threshold acuteness is formed, the crack growth is at first inhibited and eventually stops. These phenomena are virtually absent in the UEL model.

The preceding item 1 is a feature of stress distribution in the vicinity of the crack in the UMAT model and its effect would be perceptible only in the crack initiation. Presumably, the compression block upstream can send a wave of transverse compressive stress towards the crack tip thereby delaying the crack initiation. However, as already mentioned, this effect appears to be not significant for sandwich members as the cohesive zone is of greater length than in laminated composites being of the order of 6–7 mm. The second factor, too, kicks in much later; so much so that the UMAT model can be used for a study of delamination in sandwich members if one is investigating relatively small crack extensions.

Static and Dynamic Delamination in Sandwich Columns

In this section, we study the response of a compressed column when subjected to a sudden delamination of certain length. The compression carried by the column is small relative to the buckling load of the column. Because of sudden loss of equilibrium, the column exhibits a dynamic response as it adjusts itself to the new

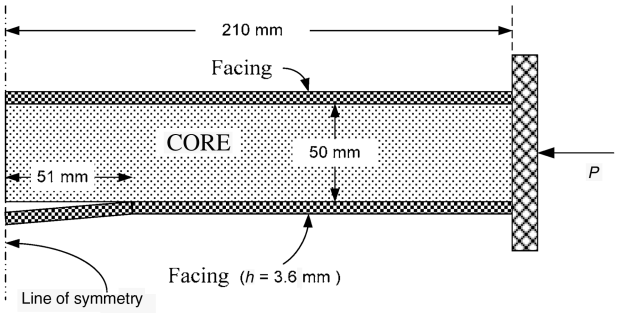

Fig. 10 Sandwich column under compression: case 1.

situation and significant additional growth of delamination occurs. We note that the static part of the problem was studied by El-Sayed and Sridharan [14] (2002) using a variant of the present UMAT model. The present study uses the UEL model for the problem and it is felt necessary to briefly summarize the salient features of the static response to assess the adverse effects of dynamic delamination. Two cases are considered: the first one is that of a relatively stout column with relatively thick facing sheets and the second is that of a slender column having very thin facing sheets.

Case 1

Geometry, Materials, and Boundary Conditions

Figure 10 shows the geometry of the specimen investigated. The core and facing materials are exactly the same as the test specimen (Table 1) discussed in the last section and the cross section of the member investigated is also the same (d = 50 mm, h = 3.6 mm). The total length of the column investigated is 420 mm and it is considered clamped at either end. Because of symmetry involved (barring the unlikely scenario of sudden interference of antisymmetric modes of bifurcation) only half the column length of 210 mm included between the line of symmetry on the left and the clamped end on the right is considered. The clamped end is modeled as a rigid surface incapable of rotation and lateral translation. A symmetrically located initial delamination of total length 102 mm is deemed to exist between bottom facing sheet and the core. Mass density of the material of the composite facings and the core were both scaled up by a factor of 10^3 to mimic masses that the member would carry in working condition and are assumed, respectively, to be 2.56 g/mm^3 and 0.2 g/mm^3. Mass proportional damping factor was taken as 0.1.

Details of the Analysis

Finite element mesh configuration is the same as that in Fig. 3; the size of the elements is 0.25 mm in the longitudinal direction and plane strain elements (CPE4R) with reduced integration are employed as before. Unlike the preceding example, the column is treated as having unit width (1 mm) and the load reported is that per millimeter. The load is inducted by prescribing the end-shortening (relative to the plane of symmetry). The critical value of SERR in the opening mode is once again taken as 1.27 N/mm. The value of maximum stress σ_{max} is taken as 10 MPa and δ_{np} is taken, as before, equal to 0.01 mm.

For both the static and dynamic analyses, the model was perturbed slightly by incorporating imperfections in order to keep the delamination open so as to prompt the structure towards delamination buckling and growth. To this end, a linear stability analysis without the cohesive layer was conducted and the buckling loads and modes were obtained. The first three buckling loads were found to be 562 N, 2079 N, and 3466 N, respectively. Of these, the first (Fig. 11) and the second pertain to delamination buckling; the former keeps the delamination fully open and the latter partially closed. The third mode is an overall buckling mode. It is clear that the first alone is critical and, therefore, an imperfection in the form of this mode is incorporated in the model with deflection of 0.5 mm at the center. Given the stoutness of the member (relative to the length, $L/d = 7.3$) and the magnitude of the overall buckling load, it is clear

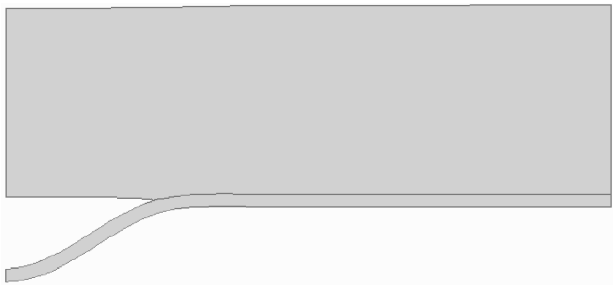

Fig. 11 The first buckling mode.

that overall bending of the column plays a relatively minor role in the problem.

Static Response

The column is compressed in a quasi-static manner, so that end-shortening increases from zero to a value at which the facings undergo an average strain of 1.5%. Nonlinearity sets in as soon as the delamination tends to buckle outward and at a load of 650 N/mm (a longitudinal stress of 90 MPa in the facing sheets) delamination begins to grow (Fig. 12). At first, this is rather rapid and occurs with little increase in load (points A, B, and C in Fig. 12), but soon settles down to a relatively modest rate and delamination occurs under increasing load thereafter. Finally, at load of 1380 N/mm (average stress of 192 MPa), a limit point is reached and, thereafter, delamination growth is accompanied by shedding of the load by the member. At a load of 1294 N/mm the delamination length recorded is 152.25 (the end-shortening = 3.15 mm).

The behavior depicted in Fig. 12 is in general agreement to that obtained by El-Sayed and Sridharan [14] in the early stages of delamination growth and, as discussed earlier, their UMAT type model tends to be stiffer and predicts a higher maximum load (not shown). Figure 12 indicates the delamination growths recorded at certain significant points in the history; in particular, the values corresponding to end -shortening magnitudes of 0.8 mm, 1.0 mm, and 1.2 mm, respectively, which are needed for comparison with those computed under dynamic delamination growth.

Dynamic Response

As mentioned earlier, the response of the sandwich column is studied in two steps. In the first step, the nodes located on the bottom facing sheet carrying the delamination are restrained from lateral (vertical) translation, thus deactivating the delamination and a certain end-shortening is applied. A static analysis is performed to model this situation. In the second step, the restraints are released suddenly while the end-shortening is kept unchanged. The sudden change in the boundary conditions results in a dynamic response, resulting in a delamination that occurs in a dynamic mode. Within duration of 0.1 s, almost complete delamination of the bottom facing sheet occurs (much more than in the corresponding static case and this is accompanied by a significant reduction in the load carried by the column).

Three cases of initially imposed end-shortening are considered. These, together with the corresponding axial loads obtained from the first step of the analysis, are as follows: 1) $\Delta = 0.8$ mm, $P = 804$ N/mm; 2) $\Delta = 1.0$ mm, $P = 1005$ N/mm; and 3) $\Delta = 1.2$ mm, $P = 1206$ N/mm. The implicit dynamic analysis available in Abaqus standard is run releasing constraints of the bottom delamination. The total duration considered was 0.1 s.

Delamination proceeds in an unstable manner under dynamic conditions. After some initial hesitation, supposedly due to inertial forces, delamination begins to occur at a fairly rapid rate with the load dropping rather abruptly. Thereafter, the rate of crack growth somewhat moderates itself. Because this is an unstable process involving rapid crack growth, the final results obtained are dictated by the size of the time increment chosen: the larger the time increment, the smaller the crack growth. The mass scaling has the effect of slowing down the response in general and delamination process in particular. Figure 13 shows the variation of current delamination length with time, obtained taking, respectively, 500, 1000, 2000, and 4000 increments over the duration of 0.1 s. For a crack growth from 51 to 100 mm, the results do exhibit a semblance of convergence with there being only minor differences in the delamination lengths given by time increments of 50 and 25 μs (2000 and 4000 increments over 0.1 s) where after the results gradually diverge. From the latter result, it is seen that the delamination attains a length of 180 mm (Fig. 13) and thus a good portion of the facing sheet (compare 180 and 210 mm) is torn away from the core. At this point, the axial load drops to 50% of the value at the end of the static phase (not shown).

It is apparent that the process of dynamic delamination is rapid with perhaps many localized vibration modes of high frequency excited. A minor factor causing the sensitivity of the delamination growth to size of the time increment is that no elements are allowed to fail during an increment (that is, from iteration to iteration). At the

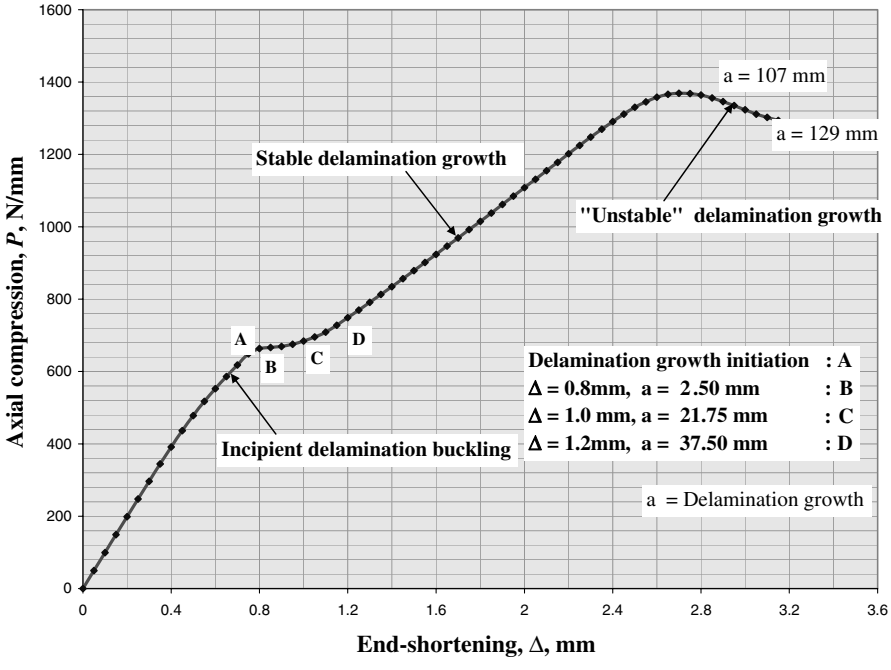

Fig. 12 Load vs end-shortening response of sandwich column under static loading, case 1.

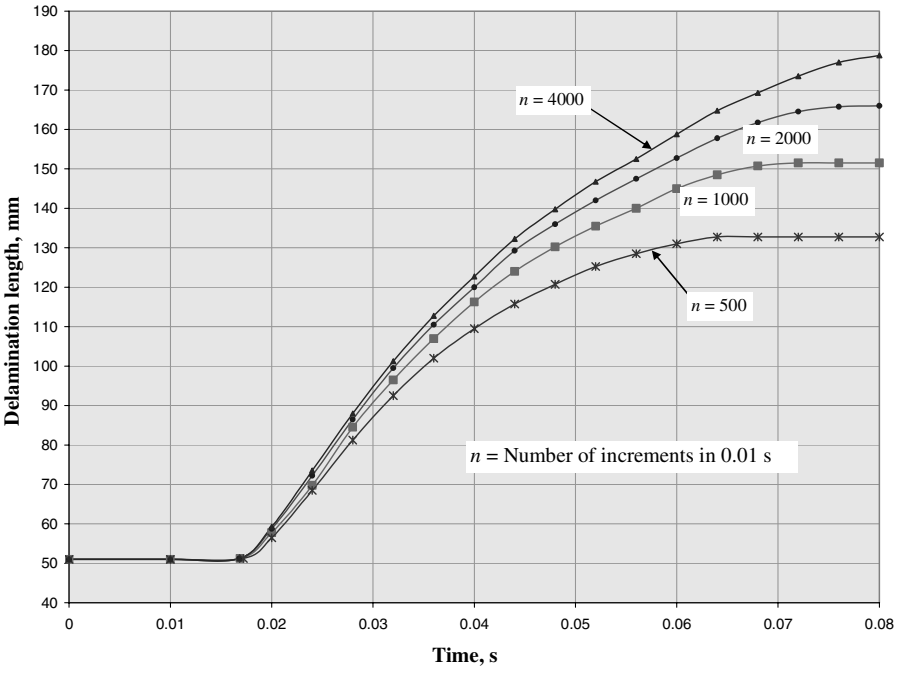

Fig. 13 Dynamic delamination, case 1: delamination length vs time for differing time increments.

end of the time increment, elements with strain energy content per unit length greater than G_{Ic} are declared to have failed. And so, a shorter time increment results in a more precise administration of the failure criterion, resulting in more elements failing in a given duration. Further, any tardiness in the failure of an element limits the deflections of the delaminated facing, which in turn slows down the growth of delamination. Thus, the error in the delamination prediction tends to get accentuated as time goes on, within a given duration.

To overcome the rather extreme sensitivity to the time increment size, a small load is applied right at the center (just as Q in Fig. 2) in lieu of the initial imperfection considered previously. This lateral load may be viewed as simulating a suction presumably due to a sudden loss of pressure in the underside of the member. The small load considered is 1% of the axial load carried at the end of the static phase applied over duration of 0.1 s at the bottom of the facing sheet at the center of the column. For the case of $\Delta = 1$ mm, the load works out to be 5 N for the half model studied.

Figure 14a and 14b show, respectively, the variation of the load supported by the column with the delamination opening measured at the center of the column and time, respectively, for the three cases of end-shortening considered. The number of increments were limited to 1000 over a duration of 0.1 s. Within a fraction of 0.1 s, the loads for all the cases considered drops to values in the range 400–550 N and the delamination of the bottom facing is almost complete. The delamination length for the case of $\Delta = 1$ mm was found to be 200 mm (cf. the total length of the column = 210 mm) at 0.08 s. The column in the deformed configuration at this stage is shown in Fig. 15. This confirms the rapidity and completeness of the dynamic delamination under compression, though the actual speed has not been established.

Case 2

We next consider a sandwich column (Fig. 16) which is significantly slender in comparison to that presented in Case 1. The column is clamped at its ends as before, the total length now is 300 mm and the total depth is 20 mm. Thus, the L/d is twice that in Case 1. Further, the thickness of the facing sheets is only 0.5 mm each and thus $d/h = 40$, again about thrice as much as in Case 1. The motivation for studying such a case is to examine the influence of overall bending and wrinkling on the delamination growth. An initial delamination of the top facing sheet of 10 mm at the center was considered (5 mm on either side of symmetry).

Both the core and facing sheets are assumed to be isotropic, for simplicity with $E_f = 26,900$ MPa, $\nu_f = 0.3$ (facings) and $E_c = 269$ MPa, $\nu_c = 0.3$ (core). Two values of G_{Ic} are considered, viz. 1.270 N/mm^2 and 0.635 N/mm^2, with $\sigma_{\max} = 6$ MPa and $\delta_o = 0.01$ mm. Once again, mass densities of the materials were scaled up and were taken as 2.5 and 0.2 g/mm^3 for facing sheet and core materials, respectively.

Finite Element Modeling

In view of the relatively small thickness of the facing sheets, modeling it with solid elements was not considered viable as the aspect ratio of the 4-noded elements needs to be maintained around unity. Therefore, it was decided to use 2-noded shear-deformable beam elements to model the facing sheets. The core was modeled using 4-noded plane stress elements (CPS4R) with reduced integration. The reference nodes of the beam elements of the top sheet were placed at the bottom of the beam section and those of the bottom sheet at the top of the section to ensure deformation compatibility with core elements. The element size along the longitudinal direction was maintained at 0.25 mm and thus there were 600 elements in each layer of elements. The aspect ratios of the core elements were kept around unity. The width of the column was taken as 1 mm, as before.

Details of Static Analysis

As before, a linear stability analysis was performed to find the critical load at which significant deformation will appear. The critical loads associated with delamination buckling and overall buckling were found to be 157.6 and 721.0 N, respectively. It is seen that as delamination buckling and growth occur, the effective center of stiffness moves downward and as a result some overall bending occurs at a fraction of the critical load associated with overall buckling predicted by linear stability analysis.

Load was introduced by prescribing end-shortening as before. The maximum end-shortening of 2 mm is selected which is about 2.5 times that corresponding to delamination buckling. Small equal and opposite loads increasing from 0 to 1 N were applied at the bottom and top nodes, respectively, at the center of the column to prompt the delamination to remain open. End-shortening was applied in small increments (1000 increments) to reach a value of 2 mm.

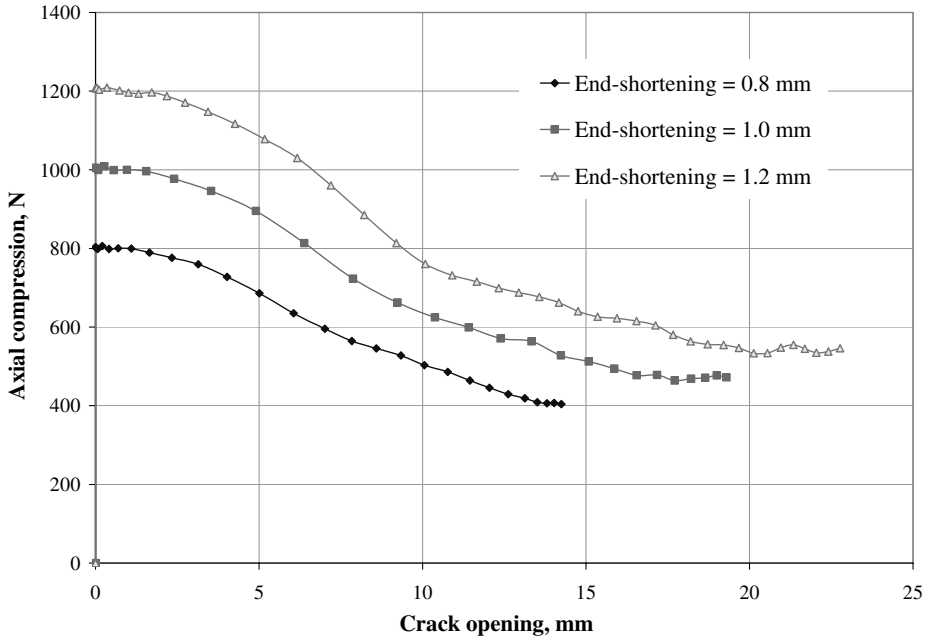

a) Dynamic response: axial compression vs delamination opening

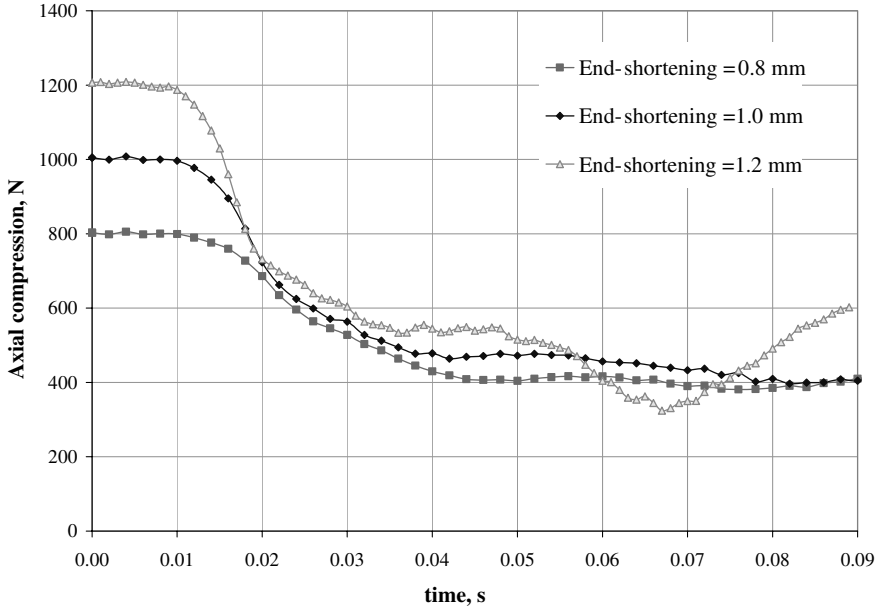

b) Axial compression vs time

Fig. 14 Dynamic response to axial compression.

Features of Static Response

Consider first the case with $G_{Ic} = 1.27$ N/mm. As the end-shortening increases to beyond the critical value, delamination occurs with about 12 elements (each 0.25 mm long) failing one after another in quick succession. The load drops slightly but thereafter recovers to increase further. During this stage, more elements fail with a total delamination growth of 9 mm when the end-shortening of 2 mm is reached. At this time, the tangential stiffness of the structure has reduced significantly with the load beginning to level off. The behavior for $G_{Ic} = 0.635$ N/mm is similar, except that delamination growth begins a little early, the load drop is more pronounced, and the total delamination growth is 18 mm. Figure 17 shows the axial compression vs end-shortening relationships.

Fig. 15 Deformed configuration for the case with end-shortening of 1 mm at t = 0.08 s.

Note, there is a significant qualitative difference between the delamination behavior under static loading of the cases 1 and 2 considered here (cf. Figs. 12 and 17). It is somewhat paradoxical to see that delamination growth is minimal for the present case of a slender column with thin facing sheets, whereas it was extensive for the case of a stouter column with thicker facing sheets. Careful examination of the deformed shape of the member as it evolves indicates that the delamination growth is influenced by overall bending of the entire column (Fig. 18) and highly localized rotation

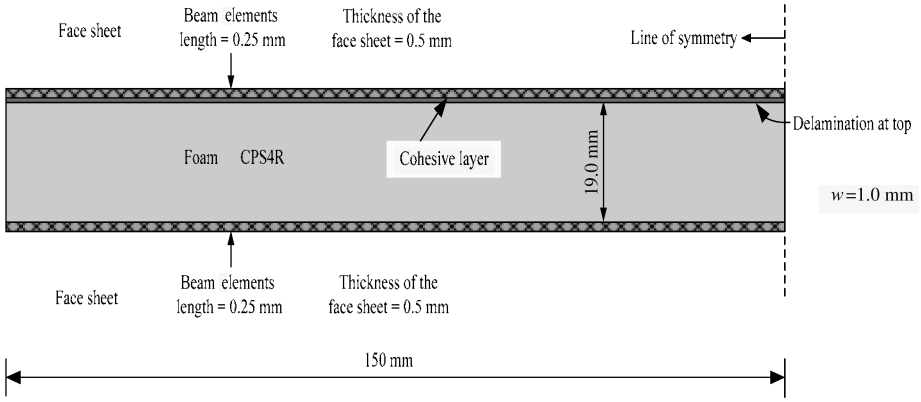

Fig. 16 Configuration of slender sandwich beam.

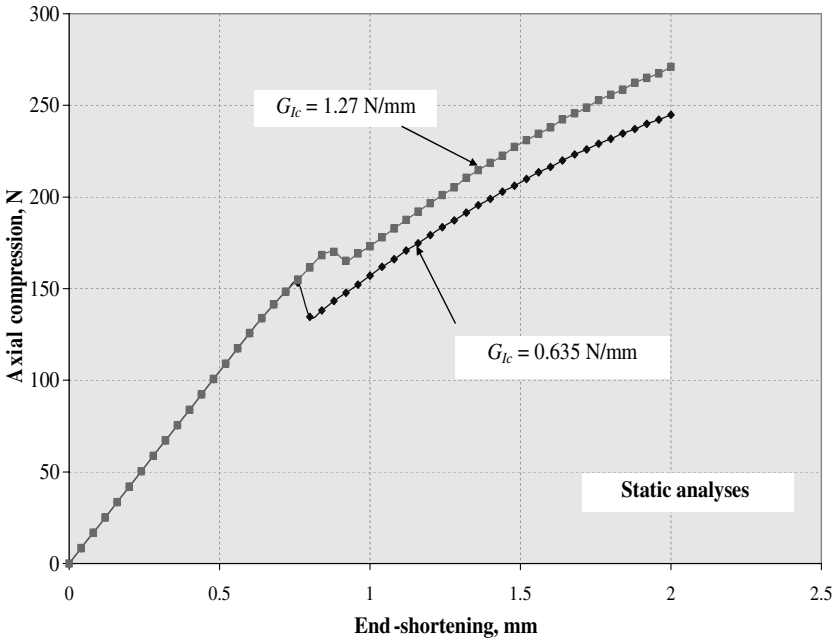

Fig. 17 Static response of sandwich column, case 2.

Fig. 18 Static response, case 2: deformed shape at end-shortening= 2 mm.

of the facing sheet that occurs at the crack tip. If the overall bending is such as to cause longitudinal tension at the facing sheet, delamination growth comes to a standstill; if it is such as to cause longitudinal compression in the delaminating facing sheet and causes the facing to bend away from the core, the portion of the facing in the vicinity of the crack tip tends to rotate and come into contact with the core, inhibiting delamination growth. Thus, we may conclude the delamination growth is not a significant factor in a slender sandwich column having thin facings under static loading. To be realistic, however, one has to consider what happens when dynamic response is triggered.

Dynamic Delamination

A loading sequence similar to that in case 1 is employed. The member is compressed to an end-shortening of 2 mm with respect to the plane of symmetry in a quasi-static mode, while the nodes along the bottom facing are restrained to prevent the opening of the delamination. In the next phase, these restraints are removed and small, equal, and opposite forces of 1 N are applied at the top and bottom center nodes, acting away from each other. The duration considered is 0.1 s.

As in the static case 2, values of G_{Ic} were considered, viz. 0.635 and 1.27 N/mm. In both the cases, delamination developed from the support as well as from the delamination tip near the center. The opening of delamination near the support was not anticipated and is apparently due to the facing sheet buckling in a wavy form similar to a column on elastic foundation, pulling the facing away from the core near the support. This is illustrated in Fig. 19 showing the deformed configuration at a point before complete delamination. Depending upon the size of the time increment selected, at the end of 0.1 s, either there was almost complete delamination of the top sheet from the core or an incomplete delamination with a relatively small portion between the two delamination fronts remaining intact. The parts of the delaminated sheet came into intermittent contact with the core during the dynamic response.

As indicated already and as in case 1 considered earlier, the prediction of the extent of the growth of delamination was found to depend on the size of the time increment chosen. Consider the case with $G_{Ic} = 1.27$ N/mm. Designate the initial delamination tip location as point A and the extent of delamination proceeding from A

Fig. 19 Case 2: dynamic delamination deformed shape for the case with $G_{Ic} = 1.27$ N/mm, t = 0.016 s; total inc = 7000.

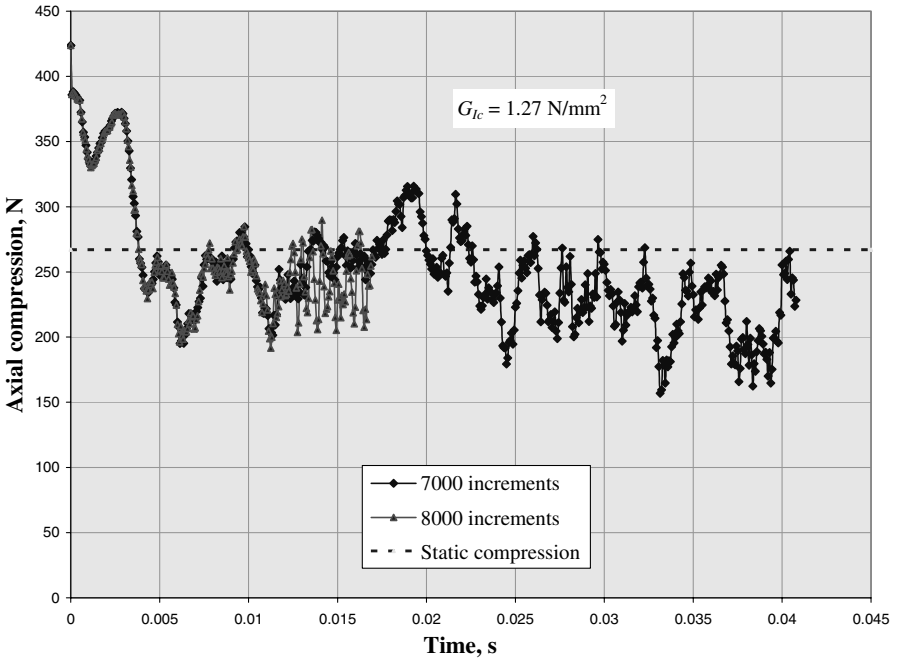

Fig. 20 Variation of the axial reaction force with time for the case with $G_{Ic} = 1.27$ N/mm.

to the left as AB; likewise, designate the left support as point P and the extent of delamination proceeding from P as PQ (Fig. 19). It is seen that both AB and PQ varied significantly with the time increment selected and this is illustrated in Table 2.

Sensitivity to increment size is typified by the significant differences in delamination growth predicted by analyses with 1000 and 5000 increments, respectively, over a duration of 0.1 sec. For 7000 and 8000 increments, even though the entire sheet is delaminated, the rates of delamination were noticeably different, with complete delamination of the top facing occurring, respectively, at 0.026 and 0.015 s, respectively.

Figure 20 shows the variation of the axial reaction force with time for the case with $G_{Ic} = 1.27$ N/mm with two different time increment sizes. The load is initially at a relatively high value (425 N) but as the delamination becomes active and grows, it drops abruptly to low values (of the order 200 N) in about 0.016 s for either case. For the case with 7000 increments, the delamination growth at this time is relative small (Fig. 19), but complete delamination occurs as indicated in Table 2 at 0.026 s (also see Fig. 21) and thereafter the load oscillates mostly between 250 to 150 N with its mean value noticeably below the value attained under static compression, viz. 267 N.

Table 2 Effect of time increment size on the extent of delamination ($G_{Ic} = 1.27$ N/mm)

Number of increments over 0.1 s	AB, mm	PQ, mm
1000	26.25	24.25
2000	33.25	25.00
5000	47.25	28.50
7000	Entire top sheet is delaminated (145 mm) in 0.026 s	
8000	Entire top sheet is delaminated (145 mm) in 0.015 s	

Conclusions

The delamination phenomena in sandwich members are studied using cohesive layer models, designated as UMAT and UEL models. When applied to a test case, it was found that the UMAT model, which has a finite thickness, can predict the initiation of delamination growth as well as some growth of delamination, but is unable to trace a large delamination growth due to an inherent deficiency. The UEL model, which has zero initial thickness, is capable of tracing the entire delamination history. Apart from the critical value of strain energy release rate, the parameter that has significant influence on crack initiation is the strength of the cohesive model material; for sandwich delamination problems using the actual strength of the core material in conjunction with the proposed models gave satisfactory results.

Delamination under dynamic conditions was studied by triggering it suddenly in a member carrying a prescribed end-shortening. Two cases are considered, case 1 of a column which was relatively stout

Fig. 21 Deformed shape: $G_{Ic} = 1.27$ N/mm, current increment= 2800; total increment = 7000.

with relatively thick facing sheets and case 2, a slender column with thin facing sheets. The delamination under such dynamic conditions was very rapid and unstable and resulted in the complete separation of the facing sheet. The overall bending of the member (in case 2) had a significant influence in inhibiting the crack growth by virtue of contact between the facing sheet and the core in the quasi-static load application, but its influence was much smaller in the case of dynamic delamination. The kind of failure in sandwich columns found in the present study illustrates the high degree of vulnerability of sandwich construction to a sudden triggering of delamination.

References

[1] Chai, H., Knauss, W. G., and Babcock, C. D., "Observation of Damage Growth in Compressively Loaded Laminates," *Experimental Mechanics*, Vol. 23, Sept. 1983, pp. 329–337.

[2] Sridharan, S., "Displacement-Based Mode Separation of Strain Energy Release Rates for Interfacial Cracks in Bi-Material Media," *International Journal of Solids and Structures*, Vol. 38, Nos. 38–39, 2001, pp. 6787–6803.

[3] El-Sayed, S., and Sridharan, S., "Cohesive Layer Models for Predicting Delamination Growth and Crack Kinking in Sandwich Structures," *International Journal of Fracture*, Vol. 117, No. 1, Sept. 2002, pp. 63–84.

[4] Ortiz, M., and Pandolfi, A., "Finite-Deformation Irreversible Cohesive Elements for Three Dimensional Crack Propagation Analysis," *International Journal for Numerical Methods in Engineering*, Vol. 44, No. 9, 1999, pp. 1267–1282.

[5] Yu, C., "Three Dimensional Cohesive Modeling of Impact Damage of Composites," Ph.D. Thesis, California Inst. of Technology, Pasadena, CA, 2001.

[6] Alfano, G., and Crisfield, M. A., "Finite Element Interface Models for the Delamination Analysis of Laminated Composites: Mechanical and Computational Issues," *International Journal for Numerical Methods in Engineering*, Vol. 50, No. 7, 2001, pp. 1701–1736.

[7] Yupeng Li, and Srinivasan Sridharan, "Performance of Two Distinct Cohesive Layer Models for Tracking Composite Delamination," *International Journal of Fracture*, Vol. 13, Nos. 1–4, Nov. 2005, pp. 99–131.

[8] "UMAT: Define a Material's Mechanical Behavior," *ABAQUS/Standard User's Manual*, Vol. 6.3, Hibbitt, Karlsson, and Sorensen, Pawtucket, RI, 2001, pp. 24.2.30.1–24.2.30.14.

[9] "UEL: Define an Element," *ABAQUS/Standard User's Manual*, Vol. 6.3, Hibbitt, Karlsson, and Sorensen, Pawtucket, RI, 2001, pp. 24.2.19.1–24.2.19.17.

[10] Sprenger, W., Gruttman, F., and Wagner, W., "Delamination Growth Analysis in Laminated Structures with Continuum-Based 3D-Shell Elements and a Visco-Plastic Softening Model," *Computer Methods in Applied Mechanics and Engineering*, Vol. 185, 2000, pp. 123–139.

[11] Charambalides, M., Kinloch, A. J., Wang, Y., and Williams, J. G., "On the Analysis of Mixed Mode Failure," *International Journal of Fracture*, Vol. 54, No. 3, April 1992, pp. 269–291.

[12] Li, X., "Debonding Fracture of Foam Core the Tilted Sandwich Structure," Ph.D. Thesis, Florida Atlantic Univ., Boca Raton, FL, 2000.

[13] Abot, J. L., "Fabrication, Testing and Analysis of Composite Sandwich Beams," Ph.D. Thesis, Northwestern Univ., Evanston, IL, 2000.

[14] El-Sayed, S., and Sridharan, S., "Performance of a Cohesive Layer Model in the Prediction of Interfacial Crack Growth in Sandwich Beams," *Journal of Sandwich Structures and Materials*, Vol. 4, Jan. 2002, pp. 31–48.

K. Shivakumar
Associate Editor